ECS Transactions, 77 (10) 67-73 (2017)
10.1149/07710.0067ecst ©The Electrochemical Society

The Effect of (La,Sr)MnO_3 Cathode Surface Termination on Its Electronic Structure

E. A. Kotomin[1,2], R. Merkle[1], Yu. A. Mastrikov[2], M. M. Kuklja[3], J. Maier[1]

[1] Max Planck Institute for Solid State Research, Stuttgart, Germany
[2]Institute for Solid State Physics, University of Latvia, Riga, Latvia
[3]Materials Science and Engineering Department, University of Maryland, USA

$La_{1-x}Sr_xMnO_3$ (LSM) was one of the first perovskites used as SOFC cathode material. Its (001) surface has two possible terminations, LaSrO and MnO_2, with quite different properties and oxygen reduction efficiencies. To avoid effects of surface polarity and the dipole moment across the material, symmetric non-stoichiometric slabs are commonly used in theoretical calculations with identical terminating planes on its both sides. We analyzed the dependence of the electronic structure (density of states) and charge distribution (effective atomic charges and chemical bond covalency) on the slab termination and Mn ion oxidation state (controlled by the Sr content and slab nonstoichiometry).

Introduction

$La_{1-x}Sr_xMnO_3$ (LSM) was one of the first perovskites employed as an SOFC cathode material and is still used in the form of porous composites with the respective electrolyte (1,2,3,4). In our previous study (5), we analyzed oxygen adsorption, dissociation and migration on the (001) MnO_2-terminated LM surface. In pure $LaMnO_3$ (LMO), the MnO_2 (001) termination was found to be the most stable energetically, however, with an increase of Sr doping, the (La,Sr)O termination is predicted to become thermodynamically even more favorable (6).

Before considering in detail the oxygen reduction reaction on the (La,Sr)O terminated surface, we analyzed, how the electronic structure (density of states, DOS, and the effective ionic charges) depend on the particular termination and Mn ion oxidation state (controlled by the Sr content and slab nonstoichiometry). Most of previous first principles calculations on a pure LMO (001) and (110) polar surfaces focused on their surface structure and energetics; both GGA+U plane wave (7,8,9) and more accurate hybrid functionals (10,11,12,13) were employed. Many studies were restricted to the high temperature cubic phase, and only a few of them analyzed the surface electronic structure (8,9). The LSM solid solutions were calculated in a couple of papers only, using both the hybrid and GGA+U methods for the bulk properties (5,14) and surface thermodynamics (5,6).

In this paper, we study the electronic structure of both LSM terminations varying the Sr content (0; 0.25; 0.50) and thus the average Mn oxidation state. We demonstrate that this is an important parameter that should be taken into account when analyzing material

and defect properties. Its effect on oxygen adsorption and reduction reaction will be discussed in a forthcoming publication.

Method

In first principles calculations, we used the *ab initio* DFT computer code VASP 4.6.19 (15,16,17) with a plane wave basis set (PAW method (18,19)) and with the GGA-type Perdew-Wang-91 exchange-correlation potential (20) employing a cut-off energy of 400 eV and a 2×2×2 Monkhorst-Pack **k**-point mesh in the Brillouin zone (21). Spin polarized calculations of the $LaMnO_3$ bulk and the [001], [110]) surfaces are in good agreement with experiment (when available) (7). In particular, for the low-temperature orthorhombic structure, the A-type anti-ferromagnetic (AAF) configuration is the energetically most favorable, in agreement with experiment. The lattice constant of both the cubic (stable above 750 K) and orthorhombic phases exceed the experimental value by only 0.5 %. The calculated cohesive energy of 30.7 eV is close to the experimental value (31 eV).

The effective atomic charges were calculated using the Bader topological analysis (22). The calculated surface relaxation and surface energies are hardly dependent upon the magnetic configuration. For slabs, the ferromagnetic configuration has the lowest energy, hence, we performed all further calculations with collinear spins. While relevant magnetic effects (≈ 0.1 eV) are much smaller than the adsorption and migration energies under study (one to several eV), a complete neglect of spin polarization results in considerable errors in material properties. We focused here on the orthorhombic phase, which is stable below 750 K.

In the (001) surface calculations, we used symmetric 7 plane-thick orthorhombic slabs with either LaO or MnO_2 termination on both sides: LaO-MnO_2-LaO-MnO_2-LaO-MnO_2-LaO or MnO_2-LaO-MnO_2-LaO-MnO_2-LaO-MnO_2, respectively. Thus, the non-stoichiometric unit cells were $La_4Mn_3O_{10}$ and $La_3Mn_4O_{11}$. To simulate the effect of Sr doping, these unit cells were expanded in the *x,y* plane parallel to the surface by $2\sqrt{2} \times 2\sqrt{2}$ (a factor of 8) and the corresponding Sr content was x_{Sr} inserted in each $La_{1-x}Sr_xO$ layer. The periodically repeated slabs were separated by a large vacuum gap of 15.8 Å. All atomic coordinates in the slab were relaxed.

Results

We discuss here results of the calculations for the effective atomic charges and density of states (DOS) for slabs with different Sr concentrations and surface terminations.

Electronic Charge Redistribution

The effective atomic charges in LMO bulk and LSM with 25% and 50% Sr are presented in Table I. Due to a considerable covalency of the Mn-O chemical bond, their effective charges are significantly smaller than the formal charges (+3 e, -2 e), whereas the Sr charge is closer to the formal one (+2 e). Calculations for LMO and LSM

containing oxygen vacancies show that the formal Mn oxidation state affects mainly the ionic charges, while the Sr concentration hardly has any effect. The Mn magnetic spin (Sz) is in good agreement with the commonly accepted high spin Mn^{3+} configuration. It decreases with increasing Sr content as expected.

TABLE I. Composition of supercells and effective charges of ions (in e) in the LMO and LSM bulk, as well as effective charges of MnO_2 and $La_{1-x}Sr_xO$ planes in the bulk. Sz is the Mn magnetic moment (in μ_B).

x_{Sr} =	La	Sr	Mn	O	La	Sr	Mn	Sz	O	MnO_2	$La_{1-x}Sr_xO$
0	8	0	8	24	2.08		1.71	3.64	-1.27	-0.82	0.82
0.25	6	2	8	24	2.09	1.59	1.78	3.42	-1.25	-0.72	0.72
0.5	4	4	8	24	2.10	1.58	1.83	3.22	-1.22	-0.62	0.62

Table II presents the average Mn oxidation state for two terminations with varying Sr doping content. It varies considerably, depending on both the slab nonstoichiometry and dopant concentration. One of our goals is to analyze how the surface electronic structure is affected by the variation in the Mn oxidation state.

TABLE II. The formal Mn average oxidation state for bulk and two terminations of 7 plane slabs

x_{Sr}	Bulk	(La,Sr)O	MnO_2
0	+3.0	2.666	3.25
0.25	+3.25	3.00	3.437
0.50	+3.5	3.333	3.625

The effective atomic charges for MnO_2 terminated surfaces of pure and Sr doped LMO are compared in Table III. It is reasonable to compare ionic charges at surfaces and in the bulk for the same Mn oxidation state, since Sr content has no effect here. Thus, the La and Sr charges are essentially identical to the bulk values, the Mn and O charges again indicate partially covalent bonding. Formally, the MnO_2-terminated plane of Sr-free LMO carries -1e charge while the subsurface LaO layer has a formal charge of +1e. The effective atomic charges of Mn and O in the surface plane are decreased below the bulk values for the same average +3.25 Mn oxidation state (1.78 and -1.25, cf. Table I, x_{sr}=0.25) indicating an increased Mn-O bond covalency. The charge of the surface plane is similar to that of a MnO_2 plane in bulk with the same Mn oxidation state (-0.72 for +3.25, cf. Table 1). While the charge of the central LaO plane is close to the bulk value of 0.82e for LaO in LM, the subsurface LaO plane is more positive, which might be a consequence of the negatively charged MnO_2 surface plane that has no charge compensation on its vacuum side.

In a slab doped by 50% of Sr, the effective charges of Sr and La ions remain nearly the same as in the bulk. The smaller Mn and O charges compared to their (extrapolated) bulk values for a Mn oxidation state of +3.625 emphasize again a more covalent bonding character. Also, the behavior of the plane charges is similar to the x_{Sr} = 0 case. Owing to the Sr doping, the $La_{1-x}Sr_xO$ plane charges are smaller than of LaO; the MnO_2 plane charges are decreased by the corresponding higher Mn oxidation state.

We note that for LaO terminated $LaMnO_3$ (Table IV(a)), the charge of La on the surface layer is significantly less positive than in the deeper layers or bulk. While the oxidation state of La^{3+} does not change, this decreased effective charge corresponds to a more covalent character of the surface layer. Together with the more negative O charge, it further contributes to decreasing the surface dipole between the positively charged LaO and the negative subsurface MnO_2 plane. The $(La_{0.5}Sr_{0.5})O$ termination of LSM (Table

IV(b)) shows similar trends as the LaO termination of LMO; however, note that the Sr charge varies less between surface and third layer than the La charge.

TABLE III. The effective atomic and plane charges of MnO_2 terminated slabs of pure LMO (a) and Sr-doped LMO (b). T denotes the terminating plane. The last line gives the effective ion charges in bulk for the same average Mn oxidation state as in the slab, calculated from the data in Table I.

(a) x_{Sr}=0					(b) x_{Sr}=0.50				
	La	**Mn**	**O**	**plane**	**La**	**Sr**	**Mn**	**O**	**plane**
T		1.69	-1.20	-0.71			1.77	-1.14	-0.51
	2.09		-1.20	0.89	2.09	1.59		-1.18	0.66
		1.83	-1.21	-0.59			1.88	-1.16	-0.44
Central	2.08		-1.25	0.83	2.09	1.57		-1.25	0.58
Bulk	2.09	1.78	-1.25		2.10	1.58	1.85	-1.21	

TABLE IV. As table I for (La,Sr)O terminated slabs.

(a) x_{Sr}=0					(b) x_{Sr}=0.50				
	La	**Mn**	**O**	**plane**	**La**	**Sr**	**Mn**	**O**	**plane**
T	1.99		-1.34	0.64	2.00	1.57		-1.33	0.45
		1.59	-1.29	-0.99			1.78	-1.24	-0.70
	2.07		-1.30	0.77	2.09	1.58		-1.24	0.60
Central		1.69	-1.27	-0.85			1.78	-1.24	-0.70
bulk	2.07	-1.6	-1.3		2.09	1.59	1.79	-1.24	

Electronic Density of States

To properly align the electronic density of states (DOS) for slabs with different concentrations of Sr doping (Fig. 1), we used the energy of a deep O*2s* state as the common reference (similar to our previous study (23)). As a consequence, the Fermi energy decreases considerably with an increase of the Mn oxidation state as the Sr content increases (see also Fig. 2).

The DOS of the (La,Sr)O termination (Fig. 1.a) clearly shows that the top of the valence band consists of Mn t_{2g} and e_g states, partially overlapping with a broad O*2p* band, centered around 15 eV. This is in good agreement with recent publication for bulk LSM (14). Unlike the broad doubly degenerate e_g band, the three-fold degenerate t_{2g} peak is quite narrow (~1 eV). The positions and shapes of Mn and O bands in subsurface 2nd and 4th planes are very similar to those in the bulk.

The DOS of the MnO_2 terminated slabs (Fig. 1.b) demonstrates that the surface Mn t_{2g} states extend over a larger energy range (~1.5 eV) due to reduced Mn ion coordination, whereas Mn in the third plane behaves similarly to the bulk. Doping with Sr does not considerably affect this splitting, but shifts the Fermi level to lower energies as expected.

Figure 2 demonstrates the considerable (~ 2 eV) dependence of the Fermi energy (the work function) for the two terminations on the averaged Mn oxidation state. Interestingly, the slopes differ considerably, i.e. the effect for MnO_2 terminated slabs is stronger than for (La,Sr)O terminations (for much thicker slabs it is expected that these slopes approach each other). Since the O*2p* states exhibit almost no shift with termination or Sr doping (Mn oxidation state) these difference in Fermi level will influence the formation energy of oxygen vacancies (which comprises transfer of electrons from O*2p* states that vanish upon vacancy formation to the Fermi level). Thus, the quantitative knowledge of this

trend is important for a consistent interpretation of the variation in surface vacancy formation energies for different slabs. The position of the Fermi level also determines the adsorption energy of atomic and molecular oxygen species, and thus affects the oxygen reduction kinetics.

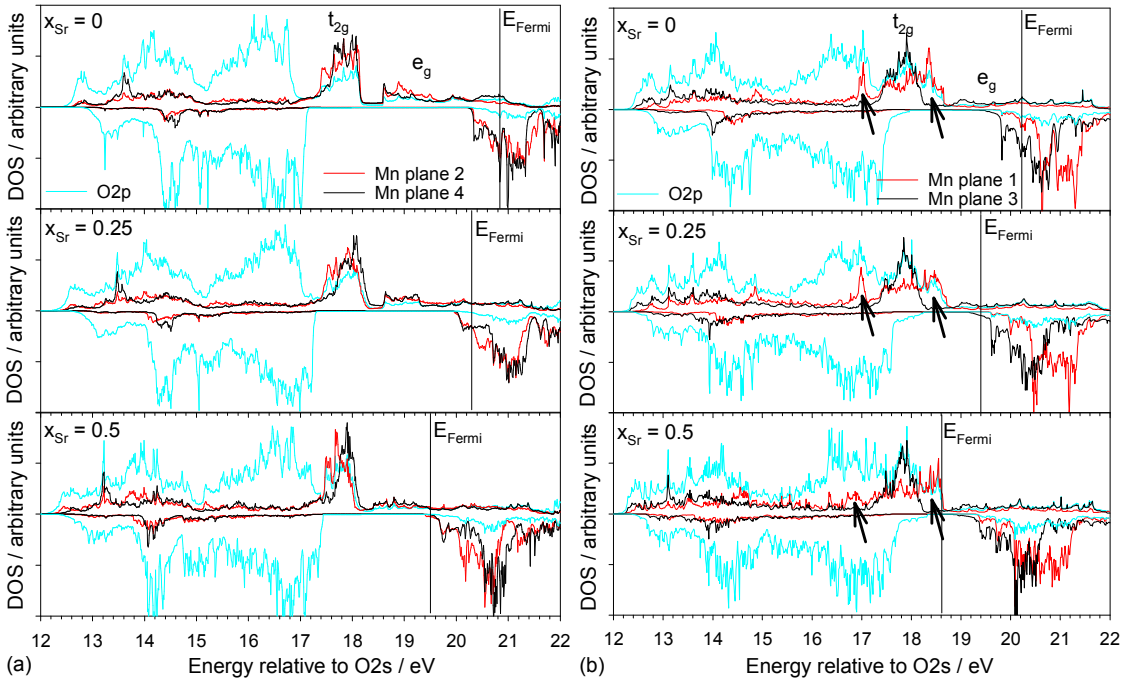

Figure 1. DOS of 7-plane $La_{1-x}Sr_xMnO_3$ slabs with different Sr content: (a) (La,Sr)O termination, (b) MnO_2 termination, the arrows in (b) indicate surface-related Mn and O states. All energy scales are fixed to E = 0 for the O*2s* state; correspondingly the position of the Fermi level varies and is indicated by the vertical lines.

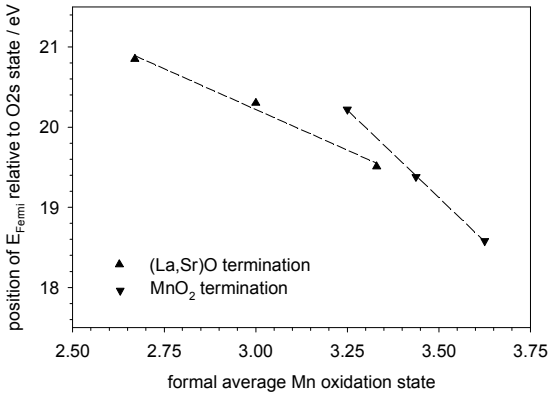

Figure 2. The position of the Fermi level relative to O*2s* states as a function of the average (formal) Mn oxidation state, for both $La_{1-x}Sr_xO$ and MnO_2 terminations.

Conclusions

The electronic structure and density of states depend considerably on the slab termination and the average oxidation state of Mn ions therein. In particular, the degenerate t_{2g} state of surface Mn ion with reduced coordination develops additional peaks, whereas deeper Mn ions behave like in the bulk. Sr doping of $LaMnO_3$ results in a

considerable shift of the Fermi level (work function) to lower energies, with the slope depending on the termination. This effect is important for the oxygen reduction kinetics on these surfaces. A considerable increase of the Mn-O bond covalency in the surface plane was observed.

Acknowledgments

This research was supported in part by DOE, NSF and the Latvian Research Program IMIS2. We used NSF XSEDE resources (Grant DMR-130077), DOE NERSC resources (Contract DE-AC02-05CH11231), computational resources at the Maryland Advanced Research Computing Center (MARCC) and at the High Performance Computer Center in Stuttgart, Germany (HLRS, project DEFTD 12939). MMK is grateful to the Office of the Director of National Science Foundation for support under the IRD program. Any appearance of findings, conclusions, or recommendations expressed in this material are those of the authors and do not necessarily reflect the views of NSF.

References

1. J. R. Wilson, J. S. Cronin, A. T. Duong, S. Rukes, H. Y. Chen, K. Thornton, D, R. Mumm, S. Barnett, *J. Pwr. Src*. **195**, 1829 (2010).
2. J. Nielsen, J. Hjelm, *Electrochim. Acta* **115**, 31 (2014).
3. M. M. Kuklja, E.A. Kotomin, R. Merkle, Yu.A. Mastrikov, J. Maier, *Phys.Chem. Chem. Phys.,* **15**, 5443 (2013).
4. E.A. Kotomin, R. Merkle, Yu.A. Mastrikov, M.M. Kuklja, J. Maier. Chapter 6 in: *Computational Approaches to Energy Materials* (eds. A. Walsh, A. Sokol, C.R.A. Catlow, Wiley), 2013, p. 149.
5. Yu.A. Mastrikov, R. Merkle, E. Heifets, E. A. Kotomin, J. Maier, *J. Phys. Chem. C* **114,** 3017 (2010).
6. S. Piskunov, E. Heifets, T. Jacob, E. A. Kotomin, E. Spohr, *Phys. Rev.* **B 78**, 121406 (2008).
7. Yu.A. Mastrikov, E. Heifets, E.A. Kotomin, J. Maier, *Surf. Sci.* **603**, 326 (2009).
8. Y.L. Lee, J. Kleis, J. Rossmeisl, D. Morgan, *Phys. Rev. B* **80**, 224101 (2009).
9. Y.L. Lee and D. Morgan, *Phys. Rev. B* **91**, 195430 (2015).
10. R.A. Evarestov, E.A. Kotomin, D. Fuks, J. Felsteiner, J. Maier, Appl. Surf. Sci., **238**, 457 (2004).
11. R.A. Evarestov, E.A. Kotomin, Yu.A. Mastrikov, D. Gryaznov, E. Heifets, J. Maier, *Phys. Rev. B* **72**, 214411 (2005).
12. E.A. Ahmad, G. Mallia, D. Kramer, A.R. Kucernak, N.M. Harrison, *J. Mater. Chem.* A **1**, 11152 (2013).
13. E.A. Ahmad, V. Tileli, D. Kramer, G. Mallia, K. Stoerzinger, Y. Shao-Horn, A.R. Kucernak, N.M. Harrison, *J. Phys. Chem. C* **119**, 16804 (2015).
14. M. Pavone, A. Munoz-Garcia, A.M. Ritzmann, E.A. Carter, *J. Phys. Chem. C* **118**, 13346 (2014).
15. G. Kresse, J. Furthmüller, *VASP the Guide*, University of Viena, Austria, 2003.
16. G. Kresse, J. Hafner, *Phys. Rev. B* **47**, 558 (1993).
17. G. Kresse, J. Furthmüller, *Phys. Rev B* **54,** 11169 (1996).

18. P.E. Bloechl, *Phys. Rev.* B **50**, 17953 (1994).
19. G. Kresse, D. Joubert, *Phys. Rev*. B **59**, 1758 (1999).
20. J.P. Perdew, J.A. Chevary, S.H. Vosko, K.A. Jackson, M.R. Pederson, D.J. Singh, C. Fiolhais, *Phys. Rev. B* **46**, 6671 (1992).
21. H.J. Monkhorst, J.D. Pack, *Phys. Rev.* B **13**, 5188 (1976).
22. G. Henkelman, A. Arnaldsson, H. Jonsson, *Comp. Mater. Sci.* **36**, 354 (2006).
23. E.A. Kotomin, Yu.A. Mastrikov, M.M. Kuklja, A.Roytburd, J.Maier, *Solid State Ionics*, **188**, 1 (2011).